A fast algorithm for a total variation based phase demodulation model.

Carlos Brito-Loeza, Ricardo Legarda-Sáenz, and Anabel Martin-González *

Abstract

In this paper we introduce fast numerical algorithms for the solution of the model [Total variation regularization cost function for demodulating phase discontinuities, Journal Applied Optics, 53(11):2297-2301, 2014]. For each variable, background illumination, amplitude modulation and phase map, we develop a fixed point method. Then, we write all three algorithms in the same framework and analyze their convergence rates, local smoothing factors by means of Local Fourier Analysis and present experimental evidence of their performance on synthetic and real world problems.

AMS subject class: 65N06, 35Q60, 65K10.

Keywords: variational methods, partial differential equations, iterative algorithms, phase demodulation, fringe patterns.

1 Introduction

Metrology is the science of measuring a given characteristic of an object or event. This characteristic may represent some physical quantities, such as size, shape, deformation, refractive index, and temperature. Applications of metrology are very important in many fields of Science and Engineering. Therefore mathematical models and efficient numerical algorithms related to this technique are in high demand.

Fringe analysis is a metrology technique for extracting measurement data from fringe patterns [40]. Measurement data can be extracted by means of phase demodulation, a process for accurately estimating the modulated

*Authors are with CLIR at Facultad de Matemáticas, Universidad Autónoma de Yucatán, México. (Emails: carlos.brito, rlegarda, amartin@correo.uady.mx; web: www.clir-lab.org)

phase from one or several fringe patterns projected over the object to be measured [33, 35].

The basic mathematical model for a fringe pattern is given by

$$I(x,y) = a(x,y) + b(x,y)\cos(\psi(x,y) + \phi(x,y)) \tag{1}$$

where $a = a(x,y)$ is the background illumination, $b = b(x,y)$ is the amplitude modulation, $\phi = \phi(x,y)$ is the phase map to be recovered and $\psi = \psi(x,y)$ the usually known spatial carrier frequency. In the literature, most methods for estimating the phase map consider it as a continuous and smooth function; see for instance the works in [23, 32] and the references therein.

Very recently however, Legarda-Saenz *et al.* [21], proposed a variational model for estimating discontinuous phase maps from a single fringe pattern. Their model was also able to estimate the background illumination and the amplitude modulation. The authors presented experimental and synthetic results showing that the new model is capable of outperforming state of the art methods in terms of the quality of the estimated phase map.

Even though the quality of reconstruction of this model is out of discussion, the model still lacks of a fast algorithm for its realization putting it in an unfavorable position in comparison to other models equipped with fast solvers. The motivation of this work, is to introduce a fast numerical algorithm to solve the optimality conditions of [21] allowing for very fast solutions.

Up to our knowledge, different uni-level methods have been tested for the task of processing fringe patterns. For instance, in [17], the authors, employed direct solvers and sparse representation for solving a two-dimensional MRI phase unwrapping problem. In [30], the phase unwrapping problem was solved using simulated annealing to remove noise in the phase map, unwrap the wrapped phase, and reconstruct the surface of the detected object. Guo *et al.* [16], proposed a total variation based model for phase unwrapping that was solved using the Split Bregman algorithm. In [45], a graph cuts-based optimization phase unwrapping algorithm was designed to solve Markov random field (MRF) model. In [25], a preconditioned conjugate gradient algorithm was used for solving a quadratic regularization functional. In [24], the authors used parallel algorithms for phase unwrapping based on MRF as well. Many methods, however, use gradient based methods [21, 38, 31, 42, 22].

The outline of this paper is as follows. In §2 we review the model to be solved and present the optimality conditions consisting on three partial

differential equations PDEs. In §3 we review the numerical solution of the PDEs, the known difficulties and introduce fixed point methods for solving each PDE. In §4, we present the numerical realization of the solvers and use §5 to analyze numerically the local smoothing factor of the fixed point algorithms by means of Local Fourier Analysis (LFA). The numerical results on both: synthetic and experimental data are presented in §6 and our conclusions are given in §7.

2 Total variation (TV) based model

In this work, we are interested in the model presented in [21], where a variational method with TV regularization to all three unknowns ϕ, a and b as shown below was presented.

$$\begin{aligned}\underset{a,b,\phi}{\arg\min}\ TV(a,b,\phi,g) \equiv \Big\{ \int_\Omega (I-g)^2 d\Omega + \frac{1}{\lambda_a}\int_\Omega |\nabla a| d\Omega \\ + \frac{1}{\lambda_b}\int_\Omega |\nabla b| d\Omega + \frac{1}{\lambda_\phi}\int_\Omega |\nabla \phi|\, d\Omega \Big\}, \end{aligned} \tag{2}$$

where $\Omega \subseteq \mathbb{R}^2$ is the domain of integration, g is a given fringe pattern, obeying the model described in (1), and $\lambda_a, \lambda_b, \lambda_\phi$ are positive regularization parameters.

As remarked in [21], this model allows the recovering of sharp phase transitions, something that other methods such as those based on L_2 regularization, fail to deliver. The model also allows to recover, at the same time, the background illumination a and the amplitude modulation b.

To get the solution of (2), its is necessary to solve the optimality conditions given by the following three partial PDEs:

$$-\nabla \cdot \frac{\nabla a}{|\nabla a|} + \lambda_a (a + b\cos(\psi+\phi) - g) = 0, \tag{3}$$

$$-\nabla \cdot \frac{\nabla b}{|\nabla b|} + \lambda_b (a + b\cos(\psi+\phi) - g)\cos(\psi+\phi) = 0, \tag{4}$$

$$-\nabla \cdot \frac{\nabla \phi}{|\nabla \phi|} + \lambda_\phi (a + b\cos(\psi+\phi) - g)(-b\sin(\psi+\phi)) = 0 \tag{5}$$

with boundary conditions

$$\frac{\partial a}{\partial \nu} = 0, \quad \frac{\partial b}{\partial \nu} = 0, \quad \frac{\partial \phi}{\partial \nu} = 0. \tag{6}$$

where ν denotes the unit outer normal to the boundary.

3 Numerical solution

As already stated in §1, most methods to process fringe patterns are lineal and therefore it suffices to use gradient based algorithms. On the contrary, the model in (2) is nonlinear. In this section, first we proceed to review the known and feasible methods for the optimality conditions and then we will move to propose ours.

A distinctive feature of the set of equations (3)-(5) is that all have an anisotropic diffusion coefficient of the form $D(u) = \frac{1}{|\nabla u|}$ (for any u). As pointed out in [7], it is known that differential equations with such type of coefficients, represent a class of challenging problems in developing fast and stable numerical algorithms. In the image processing literature, there are many examples of PDE's with similar diffusion coefficients. Maybe the most studied of them is the Euler-Lagrange equation of the total variation based image denoising model [34].

The first method we review is the very popular but very inefficient time marching method. This gradient based method is obtained by transforming each PDE into a parabolic form and then evolving it in time until reaching steady-state. For instance, by defining the left-hand side of any of the PDEs (3)-(5) as $r(u)$, we can construct the following explicit Euler method:

$$u_{i,j}^{k+1} = u_{i,j}^{k} - \Delta t \; r(u)_{i,j}^{k}, \tag{7}$$

where $k = 0, 1, \ldots$, Δt is the time-step and an initial condition $u(x, y, 0)$ is needed.

Explicit gradient descent methods used for the numerical solution of equations with similar structure to (3)-(5) are well known to have very slow convergence; see for instance [26] where a illustrative stability analysis was presented for a TV based PDE for image denoising.

It is actually quite surprising that many authors choose this method to solve their fringe pattern demodulation models, see for instance [38, 31, 42, 22]. Indeed, in [21], this method was selected to find the solution of (3)-(5) even though thousands of iterations are necessary to reach a meaningful solution.

There are ways of accelerating the convergence of the explicit Euler's method such as by multiplying $r(u)$ in (7) by $|\nabla u|$. This idea was proposed in [26] with some success but still not suitable for problems of large dimensions.

On the other hand, there is a handful of different numerical techniques to speed up computations in total variation based imaging models but most of them have not been tested for the fringe pattern demodulation problem.

For instance, the dual formulations proposed in [10, 12], the alternating minimization algorithm of [19], the semi-smooth method introduced in [27], the iterative regularization method based on Bregman distances by [28], and the fixed point method in [43] are quite efficient methods worth to try for (3)-(5). It is indeed the last method the one that we explore in this paper and show to be very reliable and fast to find the solution of (2).

In the rest of this section, we present how to construct fixed point algorithms for each PDE (3), (4), and (5).

A fixed point algorithm for a

In [5], it was recently proposed the following fixed point method for (3)

$$\left(-\nabla\cdot\frac{\nabla}{|\nabla a^k|}+\lambda_a I\right)a^{k+1}=\lambda_a(-b\cos(\psi+\phi)+g) \tag{8}$$

which results in solving at each iteration a linear system of the form

$$L_a(a^k)a^{k+1}=f_a \tag{9}$$

for $k=0,1,2,\ldots$ and where

$$f_a\equiv\lambda_a(-b\cos(\psi+\phi)+g), \tag{10}$$

$$L_a(a^k)\equiv-\nabla\cdot\frac{\nabla}{|\nabla a^k|}+\lambda_a I. \tag{11}$$

Therefore, the fixed point algorithm consists on providing a initial estimation a^0 and constructing a sequence of solutions $\{a^k\}_{k\geq 1}$ using (8). The nonlinear operator L_a is linearized by lagging the nonlinear coefficients $|\nabla a^k|^{-1}$ at every k-iteration. In this way, $L_a(a^k)$ can be shown to be symmetric, positive definite and diagonally dominant. In [5], a preconditioned conjugate gradient method (CGM) was proposed to solve the linear system.

A fixed point algorithm for b

In similar way, the following fixed point method was proposed in [5] for solving (4)

$$\left(-\nabla\cdot\frac{\nabla}{|\nabla b^k|}+\lambda_b\cos^2(\psi+\phi)\right)b^{k+1}=\lambda_b(-a+g)\cos(\psi+\phi). \tag{12}$$

where the right-hand side and linear operator are defined by

$$f_b \equiv \lambda_b(-a+g)\cos(\psi+\phi), \tag{13}$$

$$L_b(b^k) \equiv -\nabla\cdot\frac{\nabla}{|\nabla b^k|} + \lambda_b\cos^2(\psi+\phi). \tag{14}$$

Again $L_b(b^k)$ happens to be symmetric, positive definite and diagonally dominant. Hence the linear system

$$L_b(b^k)b^{k+1} = f_b \tag{15}$$

can also be solved with a preconditioned CGM or any other appropriate method for this type of systems.

A new fixed point algorithm for ϕ

Following the same ideas, a feasible fixed point method for (5) can be constructed as follows:

$$\left(-\nabla\cdot\frac{\nabla}{|\nabla\phi^k|}\right)\phi^{k+1} = -\lambda_\phi(a+b\cos(\psi+\phi^k)-g)(-b\sin(\psi+\phi^k)), \tag{16}$$

In this case, although the resultant linear system is symmetric, the operator is only semi-positive definite and weakly diagonally dominant. Therefore, convergence cannot be guaranteed for some solvers such as Jacobi, Gauss-Seidel or CG.

To fix this, we linearize the cosine function in the right hand side getting now the new fixed point iteration

$$\left(-\nabla\cdot\frac{\nabla}{|\nabla\phi^k|} + \lambda_\phi b^2\sin^2(\psi+\phi^k)\right)\phi^{k+1} =$$
$$-\lambda_\phi\sin(\psi+\phi^k)(-ab+gb-b^2(\cos(\psi+\phi^k)-\sin(\psi+\phi^k)\phi^k). \tag{17}$$

Now the system

$$L_\phi(\phi^k)\phi^{k+1} = f_\phi, \tag{18}$$

where

$$f_\phi \equiv -\lambda_\phi\sin(\psi+\phi^k)(-ab+gb-b^2(\cos(\psi+\phi^k)-\sin(\psi+\phi^k)\phi^k), \tag{19}$$

$$L_\phi(\phi^k) = -\nabla\cdot\frac{\nabla\phi^k}{|\nabla\phi^k|} + \lambda_\phi b^2\sin^2(\psi+\phi^k). \tag{20}$$

is positive definite and diagonally dominant and therefore a handful of solvers is available.

We can see (17) as a fixed point algorithm for the following problem

$$\phi^{k+1} = \min_p J(p, \phi^k) \tag{21}$$

where

$$J \equiv \int_\Omega \left(|\nabla p| + \lambda_\phi (a + b(\cos(\psi + \phi^k) - \sin(\psi + \phi^k)(p - \phi^k)) - g)^2 \right) d\Omega \tag{22}$$

Note that on the contrary to (2), $J(p, \phi^k)$ is a convex functional on p.

Finally, to compute all variables, we apply Algorithm 1

Algorithm 1 TV Algorithm

Require: $a^0, b^0, \phi^0, \nu_a, \nu_b, \nu_\phi, TOL$
  Compute $g_a = |\nabla_a TV(a^0, b^0, \phi^0)|$,
  Compute $g_b = |\nabla_b TV(a^0, b^0, \phi^0)|$,
  Compute $g_c = |\nabla_\phi TV(a^0, b^0, \phi^0)|$
  while $g_a \geq TOL$ & $g_b \geq TOL$ & $g_\phi \geq TOL$ **do**
    $a^{k+1} \leftarrow FP(a^k, f_a^k, \lambda_a, \nu_a)$
    $b^{k+1} \leftarrow FP(b^k, f_b^k, \lambda_b, \nu_b)$
    $\phi^{k+1} \leftarrow FP(\phi^k, f_\phi^k, \lambda_\phi, \nu_\phi)$
    Compute $g_a = |\nabla_a TV(a^{k+1}, b^{k+1}, \phi^{k+1})|$,
    Compute $g_b = |\nabla_b TV(a^{k+1}, b^{k+1}, \phi^{k+1})|$,
    Compute $g_c = |\nabla_\phi TV(a^{k+1}, b^{k+1}, \phi^{k+1})|$
  end while

3.1 On the convergence of the fixed point algorithms

To prove convergence of the fixed point algorithms (8), (12) and (17), it is enough to show that each one of them can be written as the generalized Weiszfeld's method. By doing this, it is possible to guarantee their global and linear convergence since these properties are inherited from the Weiszfeld's method [8].

In this section, first, we show that (8), (12) and (17) can be written in a common framework and second we show that this framework is indeed a generalized Weiszfeld's method.

To this end, we start by adopting the notation introduced in [8]. Let u be a 2-dimensional array $(u_{i,j})$ for $i = 1, \ldots, n, j = 1, \ldots, m$. We use u to represent any of the variables a, b or ϕ in (3), (4), and (5).

Let $\Omega = [0, n] \times [0, m]$ be a continuous domain and (h_x, h_y) to represent a vector of finite mesh sizes. Then the discrete domain Ω_h can be defined as $\Omega_h = \Omega \cap G_h$ where $G_h = \{(x, y) : x = x_i = ih_x, \;\; y = y_j = jh_y; \;\; i, j \in \mathbb{Z}\}$ is an infinite grid.

The discrete gradient operator $\nabla_{i,j} : \mathbb{R}^{n \times m} \to \mathbb{R}^2$ is defined as

$$\nabla_{i,j} u = \left(\frac{u_{i+1,j} - u_{i,j}}{h_x}, \frac{u_{i,j+1} - u_{i,j}}{h_y} \right).$$

and its transpose represented by $\nabla_{i,j}^T$.

Now consider the general problem

$$\min_u F(u) \equiv \sum_{i=1}^{m} \varphi(|A_i^T u|_\beta) + \frac{\lambda_u}{2} \|Ku - d\|_2^2 \tag{23}$$

where $A_i^T \in \mathbb{R}^{n \times 2}$ is a generalization of $\nabla_{i,j}^T$ and $\varphi : \mathbb{R} \to \mathbb{R}$ with $\varphi(x) = x$ in this case. Let K be a bounded linear operator and assume that [8, 39]

Hypothesis 3.1

1. *φ is C^2.*
2. *$\varphi(0) = 0$.*
3. *φ is increasing for $x \geq 0$, i.e., $\varphi'(x) > 0, x \geq 0$.*
4. *φ is convex, i.e., $\varphi''(x) > 0$.*
5. *$\upsilon(x) = \varphi(\sqrt{x})$ is concave for $x \geq 0$.*

Then

$$F'(u) = \sum_i A_i \left(\frac{\varphi'(|A_i^T u|_\beta)}{|A_i^T u|_\beta} A_i^T u \right) + \lambda_u K^*(Ku - d), \tag{24}$$

which suggests the fixed point algorithm

$$\sum_i A_i \left(\frac{\varphi'(|A_i^T u^k|_\beta)}{|A_i^T u^k|_\beta} A_i^T u^{k+1} \right) + \lambda_u K^*(Ku^{k+1} - d) = 0 \tag{25}$$

Algorithms (8), (12) and (17) can be written in the form (25) by selecting $K \in \mathbb{R}^{mn\times mn}$ and $d \in \mathbb{R}^{nm}$ as follows:

$$K_{i,j} = \begin{cases} 1 \text{ for } i = j, 0 \text{ for } i \neq j & \text{in (8)} \\ \cos(\psi_{i,j} + \phi_{i,j}) & \text{in (12)} \\ b_{i,j}\sin(\psi_{i,j} + \phi_{i,j}) & \text{in (17)} \end{cases} \tag{26}$$

$$d_{i,j} = \begin{cases} b_{i,j}\cos(\psi_{i,j} + \phi_{i,j}) - g_{i,j} & \text{in (8)} \\ a_{i,j} - g_{i,j} & \text{in (12)} \\ a_{i,j} + b_{i,j}\cos(\psi_{i,j} + \phi_{i,j}) & \\ -b_{i,j}\sin(\psi_{i,j} + \phi_{i,j})\phi_{i,j} - g_{i,j} & \text{in (17)} \end{cases} \tag{27}$$

We note that after computing d as shown in (27), we have to transform it to a column vector $d = (d_{11}, d_{1,2}, \ldots, d_{i,j}, \ldots, d_{m,n-1}, d_{m,n})$. This finishes the first part.

Now we move to show that (25) is a form of the generalized Weiszfeld's method. To do this, we follow the techniques described in [8] and [39].

The generalized Weiszfeld's method consists on choosing a uniformly strictly convex quadratic function $G(w, u)$ approximating $F(u)$ with the following assumptions:

Hypothesis 3.2

1. $G(w, u) = F(u) + (w - u), F'(u)) + \frac{1}{2}(w - u, C(u), (w - u))$.
2. $C(u)$ *is continuous.*
3. $\lambda_{min}(C(u)) \geq \mu > 0, \forall u$.
4. $F(w) \leq G(w, u))\forall w$.

Then the generalized Weiszfeld's method can be defined by

$$u^{k+1} = \min_{w} G(w, u^k) \tag{28}$$

where for fixed u, $G(u, w)$ is C^2, coercive, bounded below and strictly convex, thus the minimum exists and can be obtained by

$$G'_w(u^{k+1}, u^k) = F'(u^k) + C(u^k)(u^{k+1} - u^k) = 0. \tag{29}$$

For the fixed point algorithm in (25) it is possible to define

$$C(u^k) = A \text{ diag } \left(\frac{\varphi'(|A_i^T u^k|_\beta)}{|A_i^T u^k|_\beta} I_2\right) A^T + \lambda_u K^* K, \tag{30}$$

with $A = [A_1, \ldots, A_m]$ and I_2 a identity 2×2 matrix. Then, using this definition of $C(u^k)$ and (24) it is not difficult to see that (25) corresponds to the iteration (29) therefore property 1 in Hypothesis 3.2 holds.

To show property 2 in Hypothesis 3.2, note that continuity of $C(u)$ is guaranteed due to $|A_i^T u^k|_\beta > 0$.

Now, property 3 is fulfilled by noticing that K is a bounded non zero linear operator, therefore we can define

$$\lambda_{min}(C(u)) = \min_{\|w\|_2=1} (w, C(u)w) \tag{31}$$

and select $\mu = \lambda_{min}(C(u))$.

Now just rest to verify property 4 in Hypothesis 3.2 which is done by the following argument: by property 1 in Hypothesis 3.2, and using (23) and (24) we have that

$$\begin{aligned}
G(w,u) - F(w) &= \sum_i \left(\varphi(|A_i^T u^k|_\beta) - \varphi(|A_i^T w^k|_\beta)\right) \\
&+ \frac{\lambda_u}{2}\left(\|Ku - d\|^2 - \|Kw - d\|^2\right) \\
&+ \sum_i \frac{\varphi'(|A_i^T u^k|_\beta)}{|A_i^T u^k|_\beta}\left(A_i^T u, A_i^T w - A_i^T u\right) \\
&+ \frac{\lambda_u}{2}\left(K^*\left(Ku - d\right), w - u\right) \\
&+ \frac{1}{2}\left(A_i^T(w-u), \sum_i \frac{\varphi'(|A_i^T u^k|_\beta)}{|A_i^T u^k|_\beta} A_i^T(w-u)\right) \\
&+ \frac{1}{2}\left(w - u, K^*K(w-u)\right) \\
&= \sum_i \Big(\varphi(|A_i^T u^k|_\beta) - \varphi(|A_i^T w^k|_\beta) \\
&+ \frac{\varphi'(|A_i^T u^k|_\beta)}{2|A_i^T u^k|_\beta}\left(|A_i^T w^k|_\beta^2 - |A_i^T u^k|_\beta^2\right)\Big)
\end{aligned} \tag{32}$$

By defining, $a = |A_i^T u^k|_\beta$ and $b = |A_i^T w^k|_\beta$, we can write (32) as

$$\varphi(a) - \varphi(b) + \frac{\varphi'(a)}{2a}(b^2 - a^2) \tag{33}$$

and by definition of υ in Hypothesis 3.1 we get

$$\upsilon(a^2) - \upsilon(b^2) + \frac{\upsilon'(a^2)}{2a}(b^2 - a^2) \tag{34}$$

and being υ a concave function we get that property 4 in Hypothesis 3.2 holds. Therefore the fixed point framework (25) is a generalized Weiszfeld's method with global and linear convergence.

Following [8], it can be shown that, given the minimum u^* of (23)

$$\lambda_k = \frac{G(u^*, u^k) - F(u^k)}{\frac{1}{2}(u^* - u^k, C(u^k)(u^* - u^k))}, \tag{35}$$

$$\Lambda = 1 - \lambda_{\min}(C(u^*)^{-1} F^{''}(u^*)) \tag{36}$$

the fixed point method (25) is linearly convergent with convergence rate at most $\sqrt{\Lambda}$ where $\lambda_k < \Lambda < 1$. The proof is straightforward and we will be omitted here.

$$y_{k+1}^2 = (F(u^{k+1}) - F(u^*)) \leq \Lambda(F(u^k) - F(u^*)) = \Lambda y_k^2 \tag{37}$$

4 Numerical realization

We proceed to outline the numerical realization of the multigrid algorithm. From now on, we assume a continuous domain $\Omega = [0, m] \times [0, n]$ and let (h_x, h_y) to represent a vector of finite mesh sizes, then we define the infinite grid by $G_h = \{(x, y) : x = x_i = ih_x,\ \ y = y_j = jh_y;\ \ i, j \in \mathbb{Z}\}$, $\Omega_h = \Omega \cap G_h$ and $u_h = u_h(x, y) = u_h(x_i, y_j) = u_h(ih_x, jh_y)$ the discrete version of any function u defined on Ω_h. Derivatives are approximated using standard forward and backward finite difference schemes

$$u_x^+ = \frac{u_{i+1,j} - u_{i,j}}{h} \tag{38}$$

$$u_x^- = \frac{u_{i,j} - u_{i-1,j}}{h} \tag{39}$$

$$u_y^+ = \frac{u_{i,j+1} - u_{i,j}}{h} \tag{40}$$

$$u_y^- = \frac{u_{i,j} - u_{i,j-1}}{h} \tag{41}$$

The nonlinear terms by

$$|\nabla u|_{i+1,j} = h/\sqrt{(u_{i+1,j} - u_{i,j})^2 + (u_{i,j+1} - u_{i,j})^2 + h^2\beta} \tag{42}$$

$$|\nabla u|_{i-1,j} = h/\sqrt{(u_{i,j} - u_{i-1,j})^2 + (u_{i-1,j+1} - u_{i-1,j})^2 + h^2\beta} \tag{43}$$

$$|\nabla u|_{i,j+1} = h/\sqrt{(u_{i+1,j} - u_{i,j})^2 + (u_{i,j+1} - u_{i,j})^2 + h^2\beta} \tag{44}$$

$$|\nabla u|_{i,j-1} = h/\sqrt{(u_{i+1,j-1} - u_{i,j-1})^2 + (u_{i,j} - u_{i,j-1})^2 + h^2\beta} \tag{45}$$

The TV operator by

$$\nabla \cdot \frac{\nabla u}{|\nabla u|_\beta} = \frac{u_x^+}{|\nabla u|_{i+1,j}} - \frac{u_x^-}{|\nabla u|_{i-1,j}} + \frac{u_y^+}{|\nabla u|_{i,j+1}} - \frac{u_y^-}{|\nabla u|_{i,j-1}} \tag{46}$$

Finally, the Neumann's boundary condition on $\partial\Omega$ is treated as

$$u_{i,0} = u_{i,1}, \;\; u_{i,n+1} = u_{i,n}, \;\; u_{0,j} = u_{1,j}, \;\; u_{m+1,j} = u_{m,j}. \tag{47}$$

We can linearize globally all fixed point algorithms by freezing the nonlinear coefficients $C_{\cdot,\cdot}$'s at the k^{th}-step to obtain the same scheme given by

$$u_{i,j}^{k+1}\mathbb{S}_{i,j}^k - u_{i+1,j}^{k+1}C_{i+1,j}^k - u_{i-1,j}^{k+1}C_{i-1,j}^k - u_{i,j+1}^{k+1}C_{i,j+1}^k - u_{i,j-1}^{k+1}C_{i,j-1}^k = f_{i,j}^k \tag{48}$$

where for instance $C_{i+1,j}^k = 1/|\nabla u^k|_{i+1,j}$ and so on, $\mathbb{S}_{i,j}^k = \lambda_u + C_{i+1,j}^k + C_{i-1,j}^k + C_{i,j+1}^k + C_{i,j-1}^k$ and similarly

$$f_{i,j}^k = \begin{cases} \lambda_a(-b\cos(\psi+\phi)+g) & \text{in (8)} \\ \lambda_b(-a+g)\cos(\psi+\phi) & \text{in (12)} \\ -\lambda_\phi(a+b\cos(\psi+\phi^k)-g)(-b\sin(\psi+\phi^k)) & \text{in (16)} \end{cases} \tag{49}$$

Note that $f_{i,j}^k$ is fixed for a and b while it changes at every iteration of ϕ.

We note that it is common practice that the resulting system $L_u(u^k)u^{k+1} = f_{i,j}^k$ does not have to be solved accurately. This is, by partially solving it with a few Gauss-Seidel (or any other iterative solver) iterations is enough for the fixed point method to converge. We will estimate later the linear convergence rate and, through Local Fourier Analysis, the smoothing factor (reduction of error high frequencies) of this method. In Algorithm 2, this process of getting a partial solution by means of some iterations of the lexicographic Gauss-Seidel method is presented.

5 Local Fourier Analysis

We already have shown that the general fixed point algorithm (25) enclosing (8), (12) and (17) have global and linear convergence inherited from the Weiszfeld's method with linear convergence rate as expressed in (37). However, it is interesting to get more insight about the performance of (25) to different frequencies of the error.

The appropriate tool for doing that is Local Fourier Analysis (LFA), a technique which allows to perform a quantitative analysis of iterative methods [1, 41]. LFA can be used in two different ways: to obtain the local

Algorithm 2 Fixed Point (FP) Algorithm $u \leftarrow FP(u, f, \lambda_u, \nu)$

for $k = 1$ to ν **do**
  Compute $C^k_{i+1,j}, C^k_{i-1,j}, C^k_{i,j+1}, C^k_{i,j-1}$
  for $q = 1$ to ζ **do**
    for $i = 1$ to m **do**
      for $j = 1$ to n **do**
        $u^{q+1}_{i,j} = \frac{u^q_{i+1,j}C^k_{i+1,j} + u^{q+1}_{i-1,j}C^k_{i-1,j} + u^q_{i,j+1}C^k_{i,j+1} + u^{q+1}_{i,j-1}C^k_{i,j-1} + f^k_{i,j}}{\lambda_u + C^k_{i+1,j} + C^k_{i-1,j} + C^k_{i,j+1} + C^k_{i,j-1}}$
      end for
    end for
  end for
end for

amplification factor or to obtain the smoothing factor of a iterative algorithm. On one hand, the local amplification factor gives information on how fast all frequencies of the error are reduced at each iteration and therefore can be used to study the rate of convergence of the algorithm. On the other hand, LFA it is also helpful to study the performance of the algorithm for reducing only the high frequencies of the error. This performance is represented by the smoothing factor which is a key value when the algorithm is used in multilevel methods such as the multigrid method.

It is worth to notice that although the main application of LFA is to evaluate the performance of an algorithm on linear problems with constant coefficients on an infinite grid, LFA is a tool that has been used to get some insight of discrete nonlinear operators; see the works of [4, 20, 1, 44, 7] and the references therein. In this work, we use LFA to study the fixed point methods (8), (12) and (16) and even though they have been designed to get the solution of nonlinear problems, they can be seen as linear algorithms for $u^{k+1}_{i,j}$ since all coefficients in Algorithm 2 are constant while iterating over q.

The way to analyze nonlinear problems with LFA implies that first boundary conditions are neglected and the discrete operator is extended to an infinite grid. In practice, this means that the values obtained through LFA that are close to the boundaries will not be used. Then, it is assumed that the nonlinear operator can be linearized locally (by freezing coefficients) and can be replaced locally by an operator with constant coefficients [41].

Therefore, amplification and smoothing factors obtained thru LFA are local, meaning that they will change as the iterative algorithm evolves. In practice, a sequence of factors is constructed and the worst value is selected to estimate the performance of the algorithm.

5.1 LFA for the fixed point methods

The local iterations of any of the FP methods (8), (12), and (16), allow the following stencil representation

$$\frac{1}{h^2}\begin{bmatrix} 0 & 0 & 0 \\ -C^k_{i-1,j} & \mathbb{S}^k_{i,j} & 0 \\ 0 & -C^k_{i,j+1} & 0 \end{bmatrix} u^{q+1} = f^k_{i,j} - \frac{1}{h^2}\begin{bmatrix} 0 & -C^k_{i,j-1} & 0 \\ 0 & 0 & -C^k_{i+1,j} \\ 0 & 0 & 0 \end{bmatrix} u^q. \tag{50}$$

with $C_{,\cdot}$ and $\mathbb{S}_{i,j}$ defined as it was done in §4.

First, we start by defining $\bar{u}_{i,j}$ as the true solution at the grid point (i,j) and the error functions $\xi^{q+1}_{i,j}$ and $\xi^q_{i,j}$ as it is usually done by $\xi^{q+1}_{i,j} = \bar{u}_{i,j} - u^{q+1}_{i,j}$ and $\xi^q_{i,j} = \bar{u}_{i,j} - u^q_{i,j}$. Then, we expand errors in Fourier components as

$$\xi^{q+1}_{i,j} = \sum_{\phi_1,\phi_2=-m/2}^{m/2} \psi^{q+1}_{\phi_1,\phi_2} e^{\boldsymbol{i}\theta_1 x/h} e^{\boldsymbol{i}\theta_2 y/h} \tag{51}$$

and

$$\xi^{q}_{i,j} = \sum_{\phi_1,\phi_2=-m/2}^{m/2} \psi^{q}_{\phi_1,\phi_2} e^{\boldsymbol{i}\theta_1 x/h} e^{\boldsymbol{i}\theta_2 y/h} \tag{52}$$

where $\boldsymbol{\theta} = (\theta_1, \theta_2) \in \Theta = (-\pi, \pi]^2$, $\theta_1 = 2\pi\phi_1/m$, $\theta_2 = 2\pi\phi_2/n$ and $\boldsymbol{i} = \sqrt{-1}$.

Based on these assumptions, we can substitute (51)-(52) into the equation in Algorithm 2 to obtain the error equation

$$-\mathbb{S}^k_{i,j}\xi^{q+1}_{i,j} + C^k_{i+1,j}\,\xi^q_{i+1,j} + C^k_{i-1,j}\,\xi^{q+1}_{i-1,j} + C^k_{i,j+1}\,\xi^q_{i,j+1} + C^k_{i,j-1}\,\xi^{q+1}_{i,j-1} = 0, \tag{53}$$

where the superscript k on the coefficients is just to indicate that they were computed (frozen) at the k^{th} outer iteration. Then, the local amplification factor is given by

$$\tilde{S}_h(\boldsymbol{\theta})_{i,j} = \frac{\left| C^k_{i+1,j}\, e^{\boldsymbol{i}\theta_1} + C^k_{i,j+1}\, e^{\boldsymbol{i}\theta_2} \right|}{\left| \mathbb{S}^k_{i,j} - C^k_{i-1,j}\, e^{-\boldsymbol{i}\theta_1} - C^k_{i,j-1}\, e^{-\boldsymbol{i}\theta_2} \right|}. \tag{54}$$

Now we can separate the analysis by computing the values

$$\rho_{i,j} = \sup\{|\tilde{S}_h(\boldsymbol{\theta})_{i,j}| : \boldsymbol{\theta} \in \Theta^{high} = [-\pi, \pi)^2\} \tag{55}$$

and

$$\mu_{i,j} = \sup\{|\tilde{S}_h(\boldsymbol{\theta})_{i,j}| : \boldsymbol{\theta} \in \Theta^{high} = [-\pi, \pi)^2 \backslash [-\frac{\pi}{2}, \frac{\pi}{2})^2\}. \tag{56}$$

We will refer to $\rho_{i,j}$ as the local amplification factor and to $\mu_{i,j}$ as the smoothing factor at points (i, j). Finally, we define

$$\bar{\rho} = \sup\{\rho_{i,j} : (i, j) \in \Omega_h\}$$
$$\bar{\mu} = \sup\{\mu_{i,j} : (i, j) \in \Omega_h\}$$

to be the local amplification factor and smoothing factor of the fixed point algorithm at the k^{th} iteration.

The value of $\bar{\rho}$ will give some insight about the convergence properties of the fixed point method while the value of $\bar{\mu}$ will provide knowledge about its smoothing properties i.e how good the algorithm is to remove the high frequency components of the error. A good smoothing factor is vital for multigrid algorithms to perform well.

There are things to consider about the usage of both factors. Recall that they are only valid locally and will vary depending on some factors: the parameters λ_u, β for instance, the values of the coefficients $C_{\cdot,\cdot}$, the smoothness of the phase map and so on. The level of confidence of the computed factors will improve as the algorithm reaches converge since, close to this point, the coefficients will start to remain constant. Overall, LFA is used to get some insight about the performance of the algorithm.

We note that for the our fixed point algorithms, we already have a way to compute the global rate of convergence hence $\bar{\rho}$, which is only local, it is of less interest to us. In §6 we will focus mainly on the smoothing factor $\bar{\mu}$

6 Results

In this section, we will shortly present and discuss some results. We start by showing the convergence rates for a^k, b^k, ϕ^k and $TV(a^k, b, \phi)$, $TV(a, b^k, \phi)$, $TV(a, b, \phi^k)$ and then move on to present LFA data gathered from some experiments to show that the fixed point methods developed are indeed good smoothers.

6.1 Test problems

To test our fixed point algorithms, we designed two synthetic problems both having jumps on each variable: phase map ϕ, background illumination a,

and amplitude modulation b. On one hand, Figure 2, shows the Test problem 1, where the phase map has a simple bowl-like shape with a squared jump. On the other hand, Figure 6 shows the Test problem 2, where the phase map has a more complicated shape having smooth and piece-wise constant regions as well as corners. Finally, our third Test problem is a real problem illustrated in Figure 9.

6.2 Convergence experiments

The results we present in this section are the convergence rates obtained by running our algorithms on the Test problem 1, however similar rate values were obtained for Test problems 2 and 3. We study here the convergence rates for u^k and $TV(\cdot,\cdot,u^k)$ for each fixed point method. We note that the convergence rate for u^k is related to that for $TV(\cdot,\cdot,u^k)$ by (37) thus it is enough to consider the convergence rate for the later.

First, we show in Figures 12, 14, and 16 that the linear convergence rates λ_a^k, λ_b^k and λ_ϕ^k (for each fixed point method) indeed converge to limits $\Gamma_a, \Gamma_b, \Gamma_\phi$ as predicted by (36). We note that a naive computational implementation of (35) may produce incorrect results since it gets ill-conditioned when $u^k \to u^*$. Therefore, to compute λ^k-linear rates, we used the same strategy as in [8] and to avoid miscalculations due to rounding errors, the rates were instead estimated by constructing a sequence of values $z^k(\beta) = TV_\beta(\cdot,\cdot,u^k) - TV_\beta(\cdot,\cdot,u^*)$ and then computing $r(\beta) = \lim_{k\to\infty} \frac{z^{k+1}}{z^k}$ where u^* is the true solution that was computed to full precision using floating point arithmetic of 64 bits with residual equal to 10^{-12}. For these experiments, the initial guess used was Gaussian white noise for all variables.

By looking at the Γ-values, we observe that for this experiment they settled to $\Gamma_a \approx 0.95$, $\Gamma_b \approx 0.95$ and $\Gamma_\phi \approx 0.93$. The worse rates for Γ_a, Γ_b maybe explained by the fact that the true solutions for a and b are simple planes with low inclination and values close to zero. Hence the operators L_a, L_b are close to being weakly diagonally dominant only.

Second, we show in Figures 11,13, and 15 the way the rate of convergence deteriorates when the parameter β is reduced. This is opposite to what was reported in [8] for a similar fixed point algorithm but it is in accordance to what has been reported in numerous articles along many years for also similar fixed point algorithms. Fortunately, in practice a value of $\beta \approx 10^{-3}$ showed to be enough to recover sharp edges.

6.3 LFA experiments

In order to evaluate experimentally the smoothing quality of the proposed fixed point methods, we carried out numerical simulations over the fringe demodulation Test problems. At each fixed point iteration, we computed $\bar{\mu}$. We let the fixed point to iterate three times and then multiply the $\bar{\mu}$-values i.e $\hat{\mu} = \bar{\mu}_1\bar{\mu}_2\bar{\mu}_3$ which will be taken as the smoothing factor of the fixed point method.

The smoothing factors for Test problems 1,2,3 are given in Table 1, for phase, background illumination and amplitude modulation respectively. The numbers in Table 1, show that with three fixed point iterations we can get a smoothing factor equivalent to that of the lexicographic Gauss-Seidel method for the Laplacian equation. Recall, that the Laplacian equation is a linear PDE while the ones being solved here are nonlinear. Therefore, non standard methods have to be used as smoothers.

Having a good smoother is a key component for the implementation of multilevel algorithms. Based on the promising results shown in Table 1, we tested the fixed point algorithm for the phase map ϕ to see its performance within a nonlinear multigrid algorithm. In Figure 17 we present the iteration history of the MG algorithm for solving the Test problem 1. It is evident that convergence of the MG algorithm is very fast as expected and few FAS-cycles are needed to reach very low residual values. The large residual reduction in the first cycle is natural since we are using Gaussian random noise as initial guess and the MG hierarchy of grids acts as a low pass filter. From the second iteration and on, the residual is reduced considerably at each MG cycle at constant rate.

Unfortunately, MG convergence for Test problems 2 and 3 was not good at all. After a carefull analysis, it was observed that transporting the corrections to the next levels (either up or down the hierarchy of grids) or approximating the nonlinear operators was not working. Our conclusion is that a geometric multigrid is not the best choice for phase demodulation problems. As part of our future work, we will test the algebraic multigrid algorithm to evaluate its performance.

6.4 Quality of reconstruction

Finally, we discuss shortly the quality of reconstruction obtained with the fixed point algorithms. Although this has been addressed in [21], we want to remark that piece-wise constant regions and sharp edges are recovered with fair precision by the model and the algorithm in both synthetic and

real world problems. This is shown in Figures 4, 8 and, 10.

7 Conclusions

In this paper we have introduced three fixed point algorithms for the solution of the Total Variation based model for demodulating phase discontinuities presented in [21]. Finding the solution of this model involves solving numerically three nonlinear and anisotropic PDE's. Although the framework of our fixed point algorithms is pretty standard, we present a theoretical analysis showing their convergence and further by means of Local Fourier analysis we gathered enough experimental evidence to show that in fact, these fixed point methods have very good smoothing properties. Early experiments showed that even the good performance of these non standard smoothers is not enough to get always convergence of a geometric multigrid algorithm. We noted that geometric multigrid suffers from approximating the nonlinear operators and corrections in the hierarchy of grids, underperforming on hard problems. Therefore a algebraic multigrid algorithm would be tested in the future.

References

[1] R.E. Alcouffe, A. Brandt, J.E. Dendy and J.W. Painter. The multigrid method for the diffusion equation with strongly discontinuous coefficients. *SIAM J. Sci. Stat. Comput.*, 2(4):430–454, 1981.

[2] Noor Badshah and Ke Chen, Multigrid method for the Chan-Vese model in variational segmentation, *Commun. Comput. Phys.*, 4(2):294–316, 2008.

[3] S. Botello, J. Marroquin, and M. Rivera. Multigrid algorithms for processing fringe-pattern images. *Appl. Opt.*, 37, 7587-7595, 1998.

[4] A. Brandt. Multi-level adaptive solutions to BVPs, *Math. Comp.*, *Math. Comput.*, 31(138):333–390, 1977.

[5] Carlos Brito-Loeza, Ricardo Legarda-Saenz, Arturo Espinosa-Romero, Anabel Martin-Gonzalez. A Mean Curvature Regularized Based Model for Demodulating Phase Maps from Fringe Patterns. *Commun. Comput. Phys.*, 24(1):27-43, 2018.

[6] Carlos Brito-Loeza, Ke Chen. Multigrid method for a modified curvature driven diffusion model for image inpainting. *Journal of Computational Mathematics*, 26(6):856-875, 2008.

[7] Carlos Brito-Loeza and Ke Chen. Multigrid Algorithm for High Order Denoising. *SIAM J. Imaging Sci.*, 3(3), 363–389, 2010.

[8] Tony F. Chan and Pep Mulet. On the Convergence of the Lagged Diffusivity Fixed Point Method in Total Variation Image Restoration. *SIAM Journal on Numerical Analysis*, 2(36), 354–367, 1999.

[9] Ke Chen. *Matrix Preconditioning Techniques and Applications*, Series: Cambridge Monographs on Applied and Computational Mathematics (No. 19), Cambridge University Press, UK, 2005.

[10] Chambolle A. An algorithm for total variation minimization and applications. *SIAM J Sci Comp*, 20:89–97, 2004.

[11] Tony F. Chan, Ke Chen and Jamylle L. Carter. Iterative methods for solving the dual formulation arising from image restoration. *Electronic Transactions on Numerical Analysis*, 26:299–311, 2007.

[12] Chan T, Golub G, Mulet P. A nonlinear primal-dual method for total variation-based image restoration. *J Math Imaging Vis*, 20:1964–1977, 1999.

[13] Oscar S. Dalmau-Cedeno, Mariano Rivera, and Ricardo Legarda-Saenz. Fast phase recovery from a single closed-fringe pattern. *Journal of the Optical Society of America A*, 25(6):1361-70, 2008.

[14] Dardyk, Gregory and Yavneh, Irad. Multigrid approach to two-dimensional phase unwrapping. *Numerical Linear Algebra with Applications.*, 11. 241 - 259. 10.1002/nla.380.

[15] C. Frohn-Schauf, S. Henn and K. Witsch . Nonlinear multigrid methods for total variation image denoising. *Computing and Visualization in Science*, 7:199–206, 2004.

[16] Guo, Rongli and Zhang, Weiguang and Liu, Rong and Duan, Cunli and Wang, Fan. Phase unwrapping in dual-wavelength digital holographic microscopy with total variation regularization. *Optics Letters*, 43(14):3449, 2018.

[17] Wei He, Ling Xia, and Feng Liu. Sparse-Representation-Based Direct Minimum L-Norm Algorithm for MRI Phase Unwrapping. *Computational and Mathematical Methods in Medicine.*, (2) :134058, 2014

[18] Lars Homke. A multigrid method for anisotropic PDE's in elastic image registration. *Numerical Linear Algebra with Applications*, 13:215–229, 2006.

[19] Huang Y, Ng M, Wen Y. A fast total variation minimization method for image restoration. *Multiscale Model Simulat*, 7(2):774–795, 2008.

[20] H. Kostler, K. Ruhnau and R. Wienands. Multigrid solution of the optical flow system using a combined diffusion- and curvature-based regularizer. *Numerical Linear Algebra with Applications*, 15:201–218, 2008.

[21] Ricardo Legarda-Saenz, Carlos Brito-Loeza, Arturo Espinosa-Romero. Total variation regularization cost function for demodulating phase discontinuities. *Applied Optics*, 53(11):2297-2301, 2014.

[22] Legarda-Saenz, Ricardo and Brito-Loeza, Carlos and Rivera, Mariano and Espinosa-Romero, Arturo. Variational method for integrating radial gradient field. *Optics and Lasers in Engineering*, 63(4):53–57, 2014.

[23] Legarda-Sáenz, Osten W, Jüptner W. Improvement of the regularized phase tracking technique for the processing of nonnormalized fringe patterns. *Appl Opt.*, 41(26):5519-26, 2002.

[24] Marroquin, Jose L. and Tapia, Maximino and Rodriguez-Vera, Ramon and Servin, Manuel. interferometric synthetic aperture radar,markov random field,phase unwrapping. *Journal of the Optical Society of America A*, 12(12):2578–2585, 1995.

[25] Marroquin, Jose L. and Rivera, Mariano. Quadratic regularization functionals for phase unwrapping. *Journal of the Optical Society of America A*, 12(11):1084-7529, 1995.

[26] A. Marquina and S. Osher. Explicit algorithms for a new time dependent model based on level set motion for nonlinear deblurring and noise removal. *SIAM J. Sci. Comput.*, 22(2):387–405, 2000.

[27] Ng M, Qi L, Tang Y, Huang Y. On semismooth Newton's methods for total variation minimization. *J Math Imaging Vis*, 27(3):265–276, 2007.

[28] Osher S, Burger M, Goldfarb D, Xu J, Yin W. An iterative regularization method for total variation based image restoration. *Multiscale Model Simulat*, 4:460–489, 2005.

[29] G. Papandreou and P. Maragos. Multigrid geometric active contour models. *IEEE Transactions on Image Processing*, 16(1):229–240, 2007.

[30] Peng, Z and Wang, X and Qian, F and Zhong, X. Phase unwrapping algorithm based on simulated annealing *Acta Optica Sinica.*, 23, 845-849, 2003.

[31] Quiroga, J. A. and Servin, M. and Marroquin, J. L. Regularized phase tracking technique for demodulation of isochromatics from a single tricolour image. *Measurement Science and Technology*, 132(1):132–140, 2002.

[32] Rivera M. Improvement of the regularized phase tracking technique for the processing of nonnormalized fringe patterns. *J Opt Soc Am A Opt Image Sci Vis.*, 22(6):1170-5, 2005.

[33] David W. Robinson, Graeme T. Reid. Interferogram Analysis, Digital Fringe Pattern Measurement Techniques *CRC Press; 1 edition*, January 1, 1993.

[34] L. I. Rudin, S. Osher, and E. Fatemi. Nonlinear total variation based noise removal algorithms. *Physica D*, 60:259–268, 1992.

[35] Rajshekhar, G. and Rastogi, Pramod. Fringe analysis: Premise and perspectives *Optics and Lasers in Engineering*, 8(50):iii-x, 2012.

[36] Joseph Savage and Ke Chen. An improved and accelerated non-linear multigrid method for total-variation denoising. *International Journal of Computer Mathematics*, 82(8):1001–1015, 2005.

[37] Joseph Savage and Ke Chen. On multigrids for solving a class of improved total variation based staircasing reduction models. *In: "Image Processing Based On Partial Differential Equations", eds. X.-C. Tai, K.-A. Lie, T.F. Chan and S. Osher*, pp.69-94, Springer-Verlag, 2006.

[38] Servin, Manuel and Marroquin, Jose Luis and Quiroga, Juan Antonio. Regularized quadrature and phase tracking from a single closed-fringe interferogram. *Journal of the Optical Society of America A*, 21(3):411–419, 2018.

[39] Yuying Shi. Convergence of Fixed Point Iteration for Modified Restoration Problems. *J Math Imaging Vis*, 32(1), 31–39, 1999.

[40] Surrel Y. Fringe Analysis. *In: Rastogi P.K. (eds) Photomechanics. Topics in Applied Physics*, vol 77. Springer, Berlin, Heidelberg, 2000.

[41] Ulrich Trottenberg, Cornelis Oosterlee, and Anton Schuller. *Multigrid*. Academic Press, 2001.

[42] Villa, J. and Servin, M. Robust profilometer for the measurement of 3-D object shapes based on a regularized phase tracker. *Optics and Lasers in Engineering*, 31(4):279–288, 1999.

[43] Vogel C, Oman M. Iteration methods for total variation denoising. *SIAM J Sci Comp*, 17:227–238, 1996.

[44] R. Wienands and W. Joppich. *Practical Fourier Analysis For Multigrid Methods.* Chapman and Hall/CRC, Florida USA, 2005.

[45] Zhang, Bin and Wei, Lideng and Li, Shuang and Hu, Qingrong. interferometric synthetic aperture radar,markov random field,phase unwrapping. *Journal of Applied Remote Sensing*, 12(03):1, 2018.

Problem	$\hat{\mu}_\phi$	$\hat{\mu}_a$	$\hat{\mu}_b$
Test Problem 1	0.705	0.681	0.673
Test Problem 2	0.756	0.733	0.691
Test Problem 3	0.742	0.721	0.687

Table 1: Results of the LFA experiments.

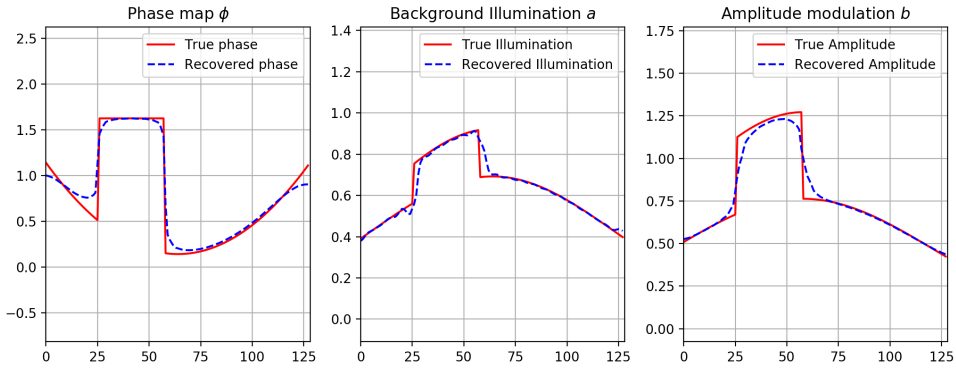

Figure 1: One line of the 2-D true and recovered variables.

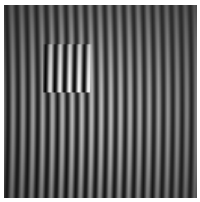

Figure 2: Fringe pattern.

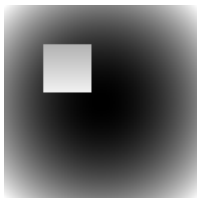

Figure 3: True phase map.

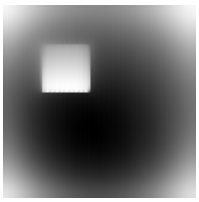

Figure 4: Recovered phase map.

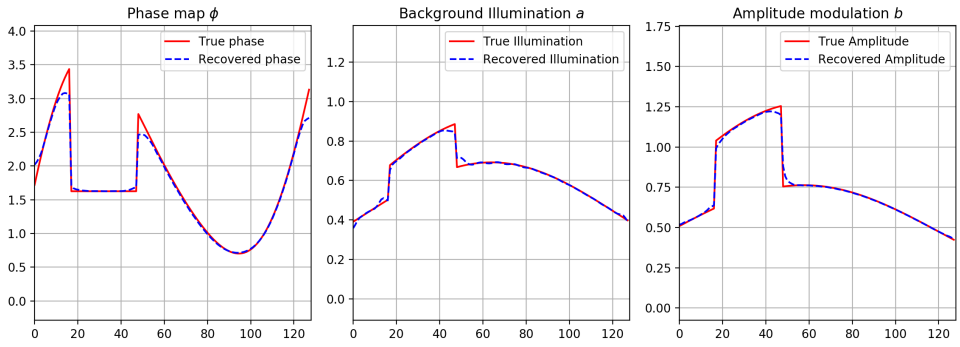

Figure 5: One line of the 2-D true and recovered variables.

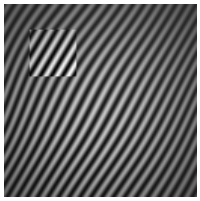

Figure 6: Fringe pattern.

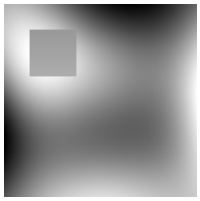

Figure 7: True phase map.

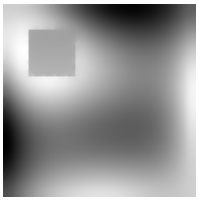

Figure 8: Recovered phase map.

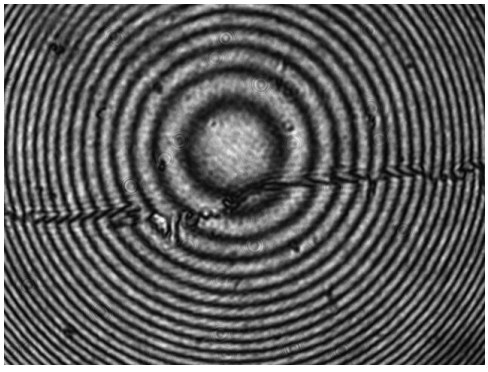

Figure 9: Experimental fringe pattern.

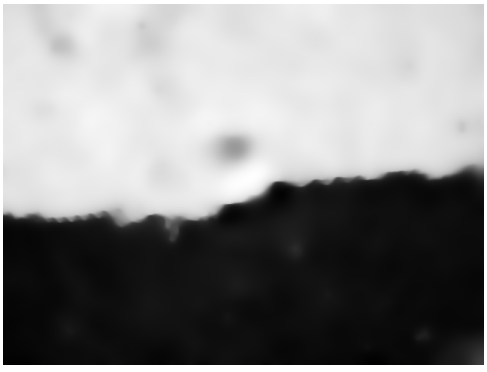

Figure 10: Estimated phase term using (2).

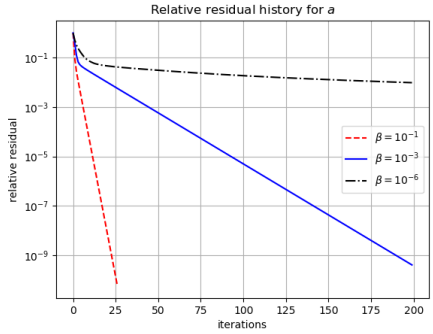

Figure 11: Residual iteration history for the background illumination variable a for the Synthetic Test problem for different values of β.

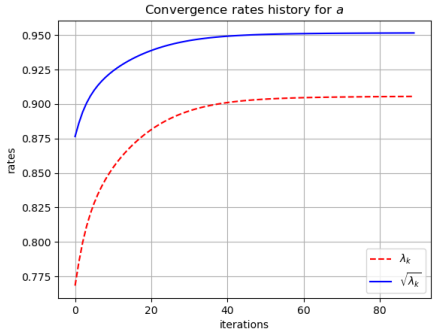

Figure 12: Convergence rates iteration history for the background illumination variable a for the Synthetic Test problem using $\beta = 0.001$.

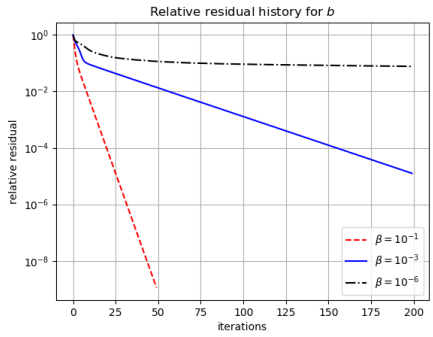

Figure 13: Residual iteration history for the amplitude modulation variable b for the Synthetic Test problem for different values of β.

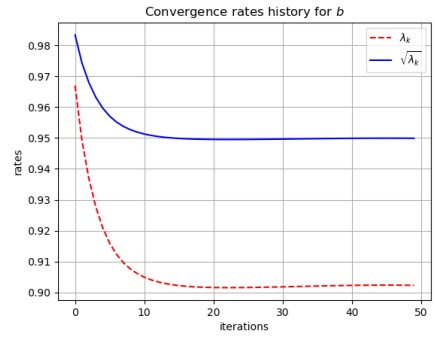

Figure 14: Convergence rates iteration history for the amplitude modulation variable b for the Synthetic Test problem using $\beta = 0.001$.

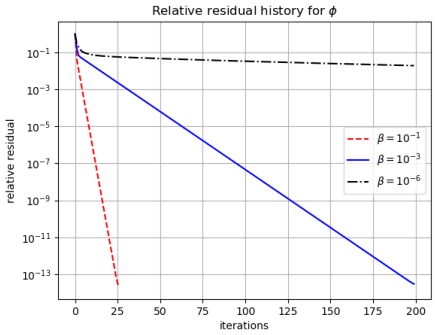

Figure 15: Residual iteration history for the phase map variable ϕ for the Synthetic Test problem for different values of β.

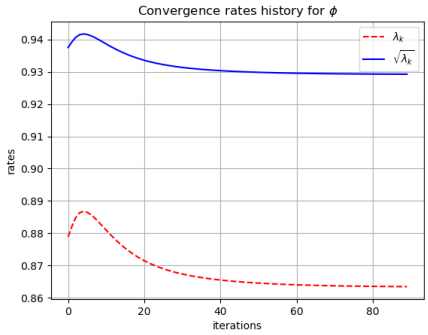

Figure 16: Convergence rates iteration history for the phase map variable ϕ the Synthetic Test problem using $\beta = 0.001$.

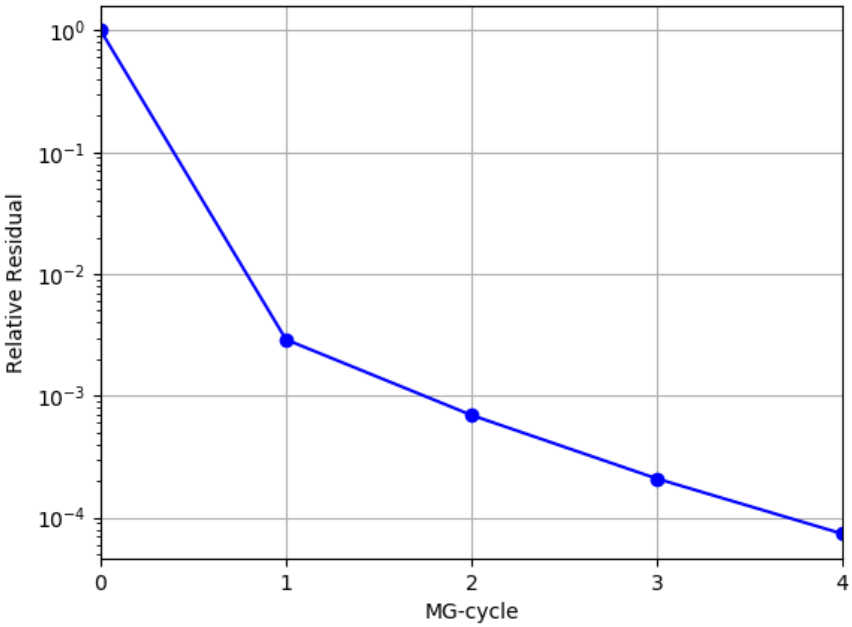

Figure 17: Multigrid algorithm cycle history for Test problem 1.